Atomically uniform Sn-rich GeSn semiconductors with 3.0-3.5 μ m room-temperature optical emission

Atomically uniform Sn-rich GeSn semiconductors with 3.0–3.5 μm room-temperature optical emission

S. Assali, J. Nicolas, S. Mukherjee, A. Dijkstra, and O. Moutanabbir

Citation: Appl. Phys. Lett. **112**, 251903 (2018); doi: 10.1063/1.5038644
View online: https://doi.org/10.1063/1.5038644
View Table of Contents: http://aip.scitation.org/toc/apl/112/25
Published by the American Institute of Physics

Atomically uniform Sn-rich GeSn semiconductors with 3.0–3.5 μm room-temperature optical emission

S. Assali,[1,a)] J. Nicolas,[1] S. Mukherjee,[1] A. Dijkstra,[2] and O. Moutanabbir[1,a)]
[1]*Department of Engineering Physics, École Polytechnique de Montréal, C. P. 6079, Succ. Centre-Ville, Montréal, Québec H3C 3A7, Canada*
[2]*Department of Applied Physics, Eindhoven University of Technology, 5600 MB Eindhoven, The Netherlands*

(Received 4 May 2018; accepted 1 June 2018; published online 19 June 2018)

The simultaneous control of lattice strain, composition, and microstructure is crucial to establish high-quality, direct bandgap GeSn semiconductors. Herein, we demonstrate that multilayer growth with a gradual increase in composition is an effective process to minimize bulk and surface segregation and eliminate phase separation during epitaxy yielding a uniform Sn incorporation up to ~18 at. %. Detailed atomistic studies using atom probe tomography reveal the presence of abrupt interfaces between monocrystalline GeSn layers with interfacial widths in the 1.5–2.5 nm range. Statistical analyses of 3-D atom-by-atom maps confirmed the absence of Sn precipitates and short-range atomic ordering. Despite the residual compressive strain of −1.3 %, the grown layers show clear room-temperature photoluminescence in the 3.0–3.5 μm wavelength range originating from the upper GeSn layer with the highest Sn content. This finding lays the groundwork to develop silicon-compatible mid-infrared photonic devices. *Published by AIP Publishing.*
https://doi.org/10.1063/1.5038644

Developing all-group IV semiconductor light emitters is an attractive approach towards the monolithic integration of photonics and electronics on the same platform.[1,2] This long-sought-for silicon photonics has recently gained revived interest motivated by pressing needs for ultrafast data transfer and low-power electronics. With this perspective, direct bandgap GeSn semiconductors have been attracting great interest for a Si-compatible processing.[3–5] Indeed, tremendous efforts have recently been expended to develop this family of group IV semiconductors, investigate their basic properties, and test their performance in a variety of optoelectronic and photonic devices.[4,6–17] The major challenge has been the control of the growth of high-quality, Sn-rich GeSn layers. In fact, achieving a direct bandgap binary alloy requires a Sn content exceeding 10 at. %, which is more than 10× the solubility of Sn in Ge.[5,18] Thus, developing these metastable semiconductors calls for a meticulous control of the growth kinetics to enhance the incorporation of Sn and prevent its segregation during growth.

The recently proposed multilayer growth has emerged as a promising approach to achieve a better control over strain and defects throughout GeSn epitaxy.[19–21] However, the observed Sn compositional gradient, resulting from the progressive strain relaxation during growth, may be undesired for the growth of heterostructures with abrupt interfaces and uniform content in each layer. Herein, we demonstrate that this limitation can be overcome by optimizing the growth process leading to GeSn layers with uniform Sn content reaching 18 at. %. By controlling the thickness and composition of two successive GeSn buffer layers with lower Sn contents, strain is progressively reduced, and a uniform incorporation of Sn is observed in the top, defect-free GeSn layer. Atom probe tomography (APT) investigations provide evidence of abrupt interfaces between GeSn layers and confirm the absence of short-range ordering and segregation of Sn. Moreover, despite the residual compressive strain in the upmost GeSn active layer, room-temperature photoluminescence (PL) emission in the 3.0–3.5 μm wavelength range is observed with typical features of band-to-band recombination.

The investigated samples were grown on 4-inch Si (100) wafers in a low-pressure CVD reactor using ultra-pure H_2 carrier gas and 10 % monogermane (GeH_4) and tin-tetrachloride ($SnCl_4$) precursors, as described in the supplementary material. A GeSn multi-layered heterostructure was grown on an ~650 nm-thick Ge/Si virtual substrate (VS), as illustrated in Fig. 1 (inset). The growth conditions were kept the same for the whole GeSn stacking, except temperature that was varied to control the incorporation of Sn. Growth

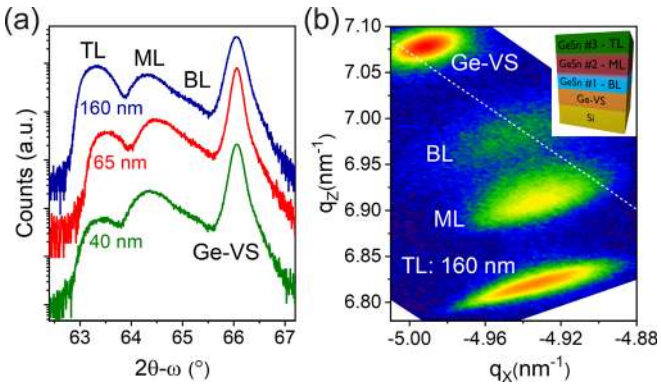

FIG. 1. (a) 2θ-ω scans around the (004) X-ray diffraction order for the 40 nm, 65 nm, and 160 nm-thick GeSn TL samples. (b) RSM around the asymmetrical (224) reflection for the 160 nm-thick TL sample. Dashed white line: line of full relaxation. Inset: schematic illustration of the GeSn multi-layer stacking grown on the Ge-VS/Si substrate.

a)Authors to whom correspondence should be addressed: simone.assali@polymtl.ca and oussama.moutanabbir@polymtl.ca

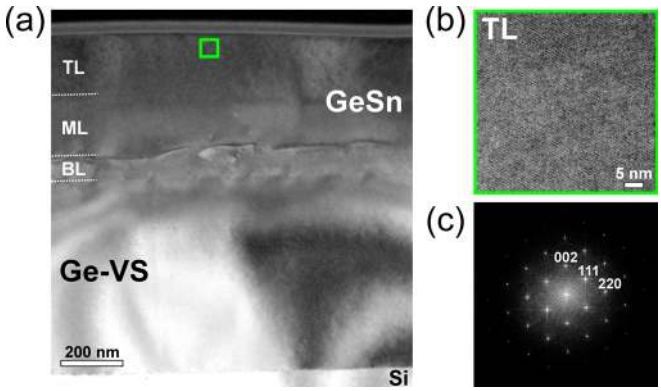

FIG. 2. (a) Cross-sectional TEM image along the [110] zone axis for the 160 nm-thick TL sample. (b) and (c) HRTEM image of the defect-free GeSn TL and corresponding indexed FFT pattern.

temperatures of 320 °C, 300 °C, and 280 °C are used for the bottom layer (BL), middle layer (ML), and top layer (TL), respectively. A growth time of 24 min and 72 min was used for BL and ML, respectively. The TL thickness was controlled by changing the growth time from 24 to 120 min, leading to a TL thickness in the 40–160 nm range as estimated using energy-dispersive X-ray spectroscopy (EDS) in a transmission electron microscope (TEM).

The crystalline quality is assessed using X-ray diffraction spectroscopy (XRD). The 2θ-ω scans around the (004) XRD order for the three samples grown with different TL thicknesses are presented in Fig. 1(a). The Ge-VS peak is detected at 66.06°, while the signal at smaller angles relates to the GeSn multi-layer stack. The TL peak is observed at 63.3°–63.5°, and it increases in intensity with the increasing TL thickness. No interference fringes are observed, indicating that the GeSn layers are partially relaxed. The ML peak at 64.3°–64.4° partially overlaps with the BL peak at ~65.0°, and their intensities are constant for all samples. The reported peak at ~65.8° associated with severe Sn segregation and precipitation[19,22,23] is not observed (see Fig. S1, supplementary material), in agreement with the APT measurements discussed below.

To decouple the effects of Sn incorporation and residual strain in the grown layers, Reciprocal Space Mapping (RSM) around the asymmetrical (224) XRD peak is performed, as shown for the 160 nm-thick GeSn TL in Fig. 1(b). The estimated Sn content, the residual strain ε, and the degree of strain relaxation R for all layers are listed in Table S1, supplementary material. In the 40 ± 5 nm-thick TL, an Sn content of 16.2 ± 0.2 at. % and a residual strain of $-1.3 \pm 0.1\%$ ($R \sim 46\%$) are estimated. When the TL thickness increases to 65 ± 5 nm, a strain value of $-1.2 \pm 0.1\%$ ($R \sim 49\%$) is measured at a Sn content of 16.1 ± 0.2 at. %. Interestingly, with a further increase in the thickness up to 160 ± 5 nm, the strain remains of $-1.3 \pm 0.1\%$ ($R \sim 47\%$) due to the increase in the Sn content reaching 17.0 ± 0.1 at. %, in agreement with the small shift to lower angles observed in Fig. 1(a). To investigate the crystalline quality and microstructure of the as-grown samples, cross-sectional TEM analyses are performed. The TEM image in Fig. 2(a) shows the GeSn TL/ML/BL stack grown on an ~650 nm-thick Ge-VS. No threading dislocations propagating toward the GeSn TL are observed, while misfit and edge dislocations are confined at the Ge-GeSn interface and within the first 100 nm of the GeSn stacking.[20,21,24] High-resolution TEM (HRTEM) image of the defect-free TL is shown in Fig. 2(b) with no additional spots in the fast-Fourier transform (FFT) image [Fig. 2(c)]. Note that an accurate evaluation threading dislocation density (TDD) lower than 1×10^7 cm^{-2} can hardly be achieved using cross-sectional TEM,[25] which can therefore be considered as an upper limit at the current stage.

To accurately evaluate the Sn content across GeSn layers, APT measurements were performed. Figure 3 exhibits the Sn profile for the 160 nm-thick TL sample, where a uniform Sn incorporation of 17.9 ± 0.2 at. % is observed in

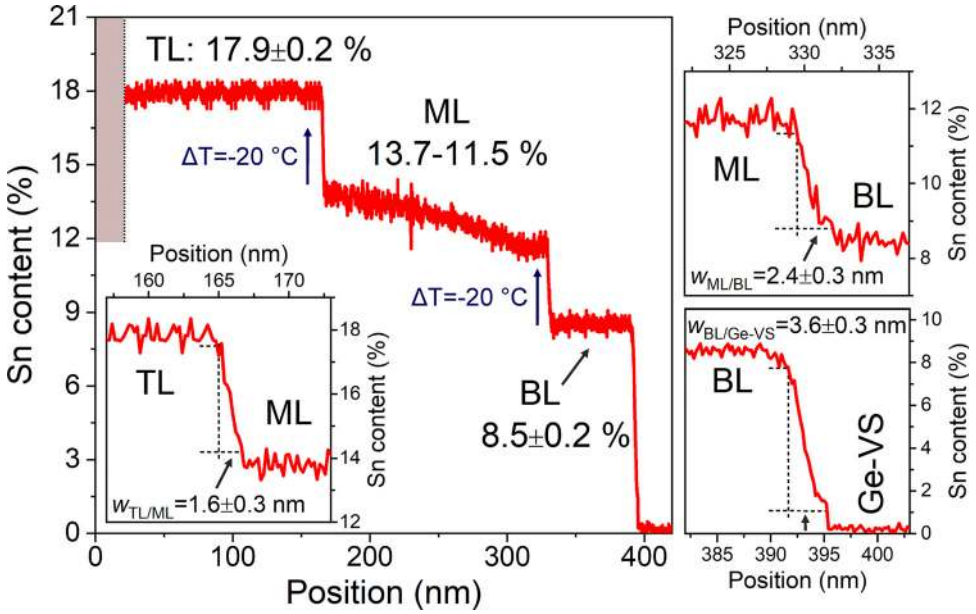

FIG. 3. APT Sn concentration profile as a function of the distance from the top surface for the 160 nm-thick TL sample. Due to evaporation instability at the tip apex, the top ~22 nm of the specimen (dashed area) is omitted. The reduction in temperature during growth ($\Delta T = -20$ °C) is indicated with dark blue arrows. Insets: zoomed-in profiles showing the heterostructure interfaces.

TL. We highlight that a homogeneous Sn composition is obtained across the TL without the presence of a compositional gradient,[19,21] indicating that the introduction of ML-BL layers enhances the strain relaxation, thus facilitating the Sn incorporation in TL. Additionally, a steep change in composition is visible at the TL/ML interface, with a decrease in the Sn content to 13.7 ± 0.2 at. % Sn. We define the width of TL/ML interface $w_{TL/ML}$ as the thickness that leads to a 90%–10% change in the APT profile intensity, as shown by the dashed lines in Fig. 3. A $w_{TL/ML} = 1.6 \pm 0.3$ nm is measured when moving across the 17.9 at. %/13.7 at. % Sn interface indicative of a sharp transition between GeSn layers. When moving away from this interface, a progressive reduction in the Sn content is visible through ML, with a slope of $\sim$14 at. %/μm, reaching 11.5% Sn in the proximity of the interface with BL. The next transition between the 11.0 at. % ML and the 8.5 at. % BL shows a $w_{ML/BL} = 2.4 \pm 0.3$ nm, while a $w_{BL/Ge\text{-}VS}$ of 3.6 ± 0.3 nm is measured for the last interface GeSn 8.5 at. % BL/Ge-VS. A temperature-dependent growth rate of 1.5 ± 0.1 nm/min, 2.4 ± 0.2 nm/min, and 2.8 ± 0.2 nm/min is estimated for TL, ML, and BL layers, respectively, hence about one order of magnitude lower than those reported in recent studies.[5,12,19,26]

Detailed insights into the short-range atomic distribution on the scale of a few lattice constants are obtained by performing a series of statistical analyses[27,28] within pre-defined $10 \times 10 \times 10\,nm^3$ regions in APT maps recorded for GeSn TL [Fig. 4(a)]. First, the frequency distribution analysis (FDA) in Fig. 4(b) shows that Ge and Sn atoms closely follow the binomial distribution, with a coefficient of determination R^2 for Ge and Sn of 0.9991 and 0.9971, respectively. This indicates that Ge and Sn are randomly distributed in the lattice.[29] Despite the Sn content being more than 18× higher than the equilibrium content,[30] not even a slight departure from an ideal solid solution is observed. To investigate further the nature of the Sn-rich GeSn lattice, partial radial distribution function (p-RDF) analysis was carried out to evaluate possible correlations between different atomic species in the alloy. Figure 4(c) shows the p-RDF of Sn with respect to (wrt) Sn within a sphere of maximum radius of 5 nm taken inside TL. The mean unity value for the p-RDF of Sn indicates that Sn atoms are completely uncorrelated wrt a given Sn atom. This behavior is characteristic of perfectly random alloys, which is in agreement with FDA [Fig. 4(b)]. These observations are also confirmed by a third set of statistical investigations evaluating the nearest-neighbor (NN) distributions in Fig. 4(d). Herein, the distance between a Sn atom and its closest neighboring Sn atoms is calculated (1st order), and then, the algorithm is extended to evaluate the correlation with the *k*th order neighbors (red curves). The results are then compared with the expected distribution for an ideal solid solution, where atoms are randomly distributed with a bulk normalized concentration (dashed black lines).[31] This agreement between experimental and theoretical APT simulations is a compelling evidence of the absence of short-range ordering effects in the grown Sn-rich alloys.[27] Finally, Fig. 4(e) displays the 7 at. % Sn iso-concentration surfaces (yellow) in a horizontal slice of the 3D APT reconstruction in Fig. 4(a). In the presence of aggregates (precipitates or clusters), this would give rise to closed surfaces bounding the aggregates.[32] On the contrary, only statistical fluctuations are observed [Fig. 4(e)], thus confirming the absence of any Sn aggregates.

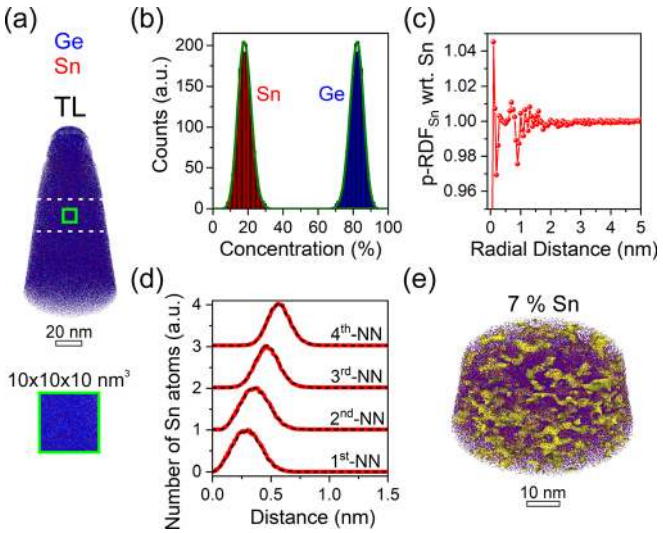

FIG. 4. (a) APT reconstructed map of the upper portion of the GeSn TL and the $10 \times 10 \times 10\,nm^3$ cube used for the statistical analysis. For clarity, only 10% of the Ge (blue) and Sn (red) atoms are shown. (b) Frequency distribution of Ge (blue) and Sn (red) in $Ge_{0.82}Sn_{0.18}$ TL (histograms) and the corresponding binomial distributions (green lines). (c) p-RDF of Sn (within TL) wrt a central Sn atom. The statistical fluctuations around the value of unity at small radii originate from the small number of Sn atoms that a small-radius sphere can encompass. (d) NN analysis for Sn atoms (red curves), which evaluates the distance between every Sn atoms and its first (to fourth) neighbors with respect to a randomized dataset for a perfect random alloy (black-dashed curves). (e) Iso-concentration surfaces (yellow) drawn at 7.0 at. % Sn concentration within TL.

To evaluate the relevance of the as-grown layers for photonic applications, the optical emission was investigated with room-temperature photoluminescence (PL) measurements using 976 nm and 405 nm excitation lasers (Figs. S2 and S3, supplementary material).[8] In the PL spectra in Fig. 5(a) for the 16.4 ± 0.4 at. % Sn (estimated with APT) samples with a 40–65 nm-thick TL, a sharp main emission peak at $\sim$0.39 eV and an additional shoulder peak at 0.43–0.44 eV are observed [solid curves in Fig. 4(a)]. A further increase in the Sn content to 17.9 ± 0.2 at. % and thickness to 160 nm induces a redshift of both peaks reaching 0.36 eV and 0.41 eV. A $\sim$50 meV energy difference between the two emission peaks is observed in all samples. In addition, a full width at half maximum of only 30–50 meV is measured for the main emission at 0.36–0.39 eV. By reducing the penetration depth of the excitation from $\sim$266 nm (976 nm laser) to $\sim$14 nm using the 405 nm laser (Fig. S3, supplementary material), no significant changes in PL spectra are observed [dashed curves in Fig. 5(a)]. An increase in the integrated PL intensity with the increasing TL thickness is estimated [Fig. 5(b)], which is independent of the excitation wavelength (Fig. S4, supplementary material). Thus, the independence of PL spectra on the penetration depth of the excitation demonstrates that the optical emission originates from TL rather than from the underlying lower Sn content layers, with a negligible effect of nonradiative surface recombination. Temperature-dependent PL measurements down to 4 K (not shown) provide further clear evidence that the optical emission originates from the TL. The residual compressive strain

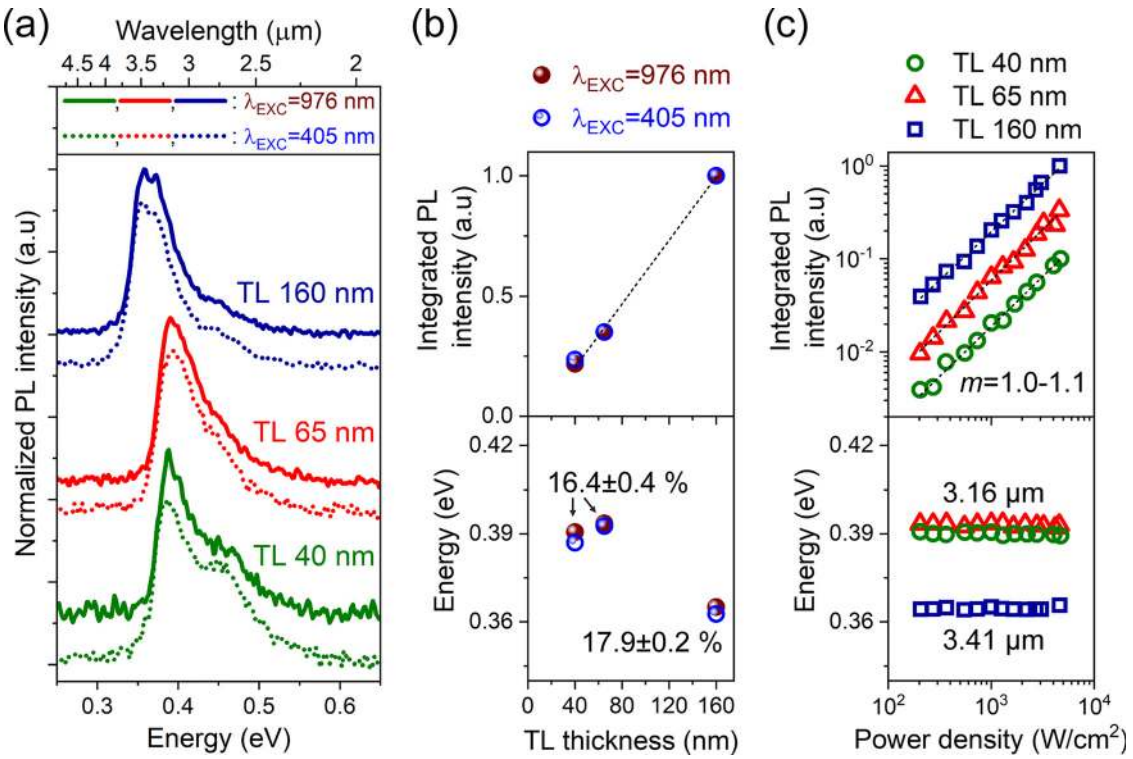

FIG. 5. (a) Room-temperature PL spectra recorded for samples with variable TL thicknesses acquired with 976 nm (solid curves) and 405 nm (dashed curves) lasers. An excitation power density below 1.0 kW/cm^2 was used. (b) Integrated PL intensity and peak energy value as a function of TL thickness for 976 nm and 405 nm excitation wavelengths. (c) Integrated PL intensity and peak energy as a function of the excitation power density (976 nm laser).

(−1.3 %) in the GeSn TL is predicted to reduce both the bandgap and the energy barrier between the Γ- and L-minimum $\Delta E_{L\Gamma}$, with a reduction of the directness of the bandgap.[18,33] However, a direct bandgap below 0.45 eV with $\Delta E_{L\Gamma}$ larger than 120 meV is predicted for 18 at. % GeSn pseudomorphically grown on a relaxed 13 at. % GeSn layer.[33] This supports the observation of room-temperature PL emission in our work at energies lower than 0.40 eV, resulting from the confinement of the optically generated carriers in TL, without the need for thick relaxed layers[12,21,26] or tensile-strain engineering[9] processes. To gain a deeper understanding of the nature of the emission, power-dependent PL measurements are performed. The integrated PL intensity (I_{PL}) shows a linear dependence on the excitation power density (P_{EXC}) for all samples [Fig. 5(c)]. The slope m∼1.0–1.1 obtained by fitting the optical data using the power law $I_{PL} \propto P_{EXC}^{m}$ together with the independence of the peak energy on the excitation power density is indicative of the band to band recombination, therefore excluding impurity-related recombination channels[34–36] and band-filling effects.[37]

In summary, we demonstrated the growth of atomically uniform, defect-free GeSn layers with Sn contents reaching a uniform composition of ∼18 at. %. Atomistic-level mapping provided clear evidence that the growth yields abrupt interfaces, with an interfacial width of 1.5–2.5 nm, across the GeSn multi-layer stacking. Moreover, APT maps confirmed the absence of Sn precipitates and short-range atomic ordering in as-grown, Sn-rich layers. Room-temperature optical emission is achieved at 0.36–0.39 eV despite the residual compressive strain of −1.3 %. This 3.0–3.5 μm emission band is obtained with an ∼1.1 μm-thick GeSn/Ge-VS multi-layer stacking that is approaching the thickness requirement for monolithically integrated mid-IR photonics.[38–40] Furthermore, the sharp interfaces across GeSn layers pave the way for a better control of the growth of GeSn-based multi-quantum wells and heterostructures for emission sources and detectors with a broad spectral tunability.[41–45]

See supplementary material for additional information on the growth conditions, XRD-RSM characterization, and PL setup and measurements.

The authors thank É. Bouthillier and A. Attiaoui for the fruitful discussions and J. Bouchard for the technical support with the CVD system. O.M. acknowledges support from NSERC Canada (Discovery, SPG, and CRD Grants), Canada Research Chair, Canada Foundation for Innovation, Mitacs, and MRIF Québec. A.D. acknowledges support from the NWO gravity program.

The authors declare no competing financial interest.

[1]*Silicon Photonics III: Systems and Applications*, edited by L. Pavesi and D. J. Lockwood (Springer Berlin Heidelberg, Berlin, Heidelberg, 2016).
[2]R. Soref, D. Buca, and S.-Q. Yu, Opt. Photonics News **27**, 32 (2016).
[3]J. Kouvetakis, J. Mathews, R. Roucka, A. V. G. Chizmeshya, J. Tolle, and J. Menendez, IEEE Photonics J. **2**, 924 (2010).
[4]D. Stange, S. Wirths, R. Geiger, C. Schulte-Braucks, B. Marzban, N. V. Den Driesch, G. Mussler, T. Zabel, T. Stoica, J.-M. Hartmann, S. Mantl, Z. Ikonic, D. Grützmacher, H. Sigg, J. Witzens, and D. Buca, ACS Photonics **3**, 1279 (2016).
[5]S. Wirths, R. Geiger, N. V. Den Driesch, G. Mussler, T. Stoica, S. Mantl, Z. Ikonic, M. Luysberg, S. Chiussi, J. M. Hartmann, H. Sigg, J. Faist, D. Buca, and D. Grützmacher, Nat. Photonics **9**, 88 (2015).
[6]D. Stange, S. Wirths, N. Von Den Driesch, G. Mussler, T. Stoica, Z. Ikonic, J. M. Hartmann, S. Mantl, D. Grützmacher, and D. Buca, ACS Photonics **2**, 1539 (2015).

[7]J. Werner, M. Oehme, M. Schmid, M. Kaschel, A. Schirmer, E. Kasper, and J. Schulze, Appl. Phys. Lett. **98**, 061108 (2011).
[8]S. Assali, A. Dijkstra, A. Li, S. Koelling, M. A. Verheijen, L. Gagliano, N. von den Driesch, D. Buca, P. M. Koenraad, J. E. M. Haverkort, and E. P. A. M. Bakkers, Nano Lett. **17**, 1538 (2017).
[9]R. W. Millar, D. C. S. Dumas, K. F. Gallacher, P. Jahandar, C. MacGregor, M. Myronov, and D. J. Paul, Opt. Express **25**, 25374 (2017).
[10]A. Gassenq, L. Milord, J. Aubin, N. Pauc, K. Guilloy, J. Rothman, D. Rouchon, A. Chelnokov, J. M. Hartmann, V. Reboud, and V. Calvo, Appl. Phys. Lett. **110**, 112101 (2017).
[11]R. Loo, B. Vincent, F. Gencarelli, C. Merckling, A. Kumar, G. Eneman, L. Witters, W. Vandervorst, M. Caymax, M. Heyns, and A. Thean, ECS J. Solid State Sci. Technol. **2**, N35 (2012).
[12]V. Reboud, A. Gassenq, N. Pauc, J. Aubin, L. Milord, Q. M. Thai, M. Bertrand, K. Guilloy, D. Rouchon, J. Rothman, T. Zabel, F. Armand Pilon, H. Sigg, A. Chelnokov, J. M. Hartmann, and V. Calvo, Appl. Phys. Lett. **111**, 092101 (2017).
[13]S. Al-Kabi, S. A. Ghetmiri, J. Margetis, W. Du, A. Mosleh, W. Dou, G. Sun, R. A. Soref, J. Tolle, B. Li, M. Mortazavi, H. A. Naseem, and S.-Q. Yu, J. Electron. Mater. **45**, 6251 (2016).
[14]J. D. Gallagher, C. L. Senaratne, P. M. Wallace, J. Menendez, and J. Kouvetakis, Appl. Phys. Lett. **107**, 123507 (2015).
[15]N. Taoka, G. Capellini, V. Schlykow, M. Montanari, P. Zaumseil, O. Nakatsuka, S. Zaima, and T. Schroeder, Mater. Sci. Semicond. Process. **70**, 139 (2017).
[16]W. Wang, Q. Zhou, Y. Dong, E. S. Tok, and Y.-C. Yeo, Appl. Phys. Lett. **106**, 232106 (2015).
[17]S. Zaima, O. Nakatsuka, N. Taoka, M. Kurosawa, W. Takeuchi, and M. Sakashita, Sci. Technol. Adv. Mater. **16**, 043502 (2015).
[18]A. Attiaoui and O. Moutanabbir, J. Appl. Phys. **116**, 063712 (2014).
[19]J. Aubin, J. M. Hartmann, A. Gassenq, J. L. Rouviere, E. Robin, V. Delaye, D. Cooper, N. Mollard, V. Reboud, and V. Calvo, Semicond. Sci. Technol. **32**, 094006 (2017).
[20]J. Margetis, S.-Q. Yu, N. Bhargava, B. Li, W. Du, and J. Tolle, Semicond. Sci. Technol. **32**, 124006 (2017).
[21]W. Dou, M. Benamara, A. Mosleh, J. Margetis, P. Grant, Y. Zhou, S. Al-Kabi, W. Du, J. Tolle, B. Li, M. Mortazavi, and S.-Q. Yu, Sci. Rep. **8**, 5640 (2018).
[22]J. Aubin, J. M. Hartmann, A. Gassenq, L. Milord, N. Pauc, V. Reboud, and V. Calvo, J. Cryst. Growth **473**, 20 (2017).
[23]D. Weisshaupt, P. Jahandar, G. Colston, P. Allred, J. Schulze, and M. Myronov, in *2017 40th International Convention on Information Communication Technology Electronics and Microelectronics* (IEEE, 2017), pp. 43–47.
[24]S. Takeuchi, A. Sakai, O. Nakatsuka, M. Ogawa, and S. Zaima, Thin Solid Films **517**, 159 (2008).
[25]Y. Yamamoto, P. Zaumseil, T. Arguirov, M. Kittler, and B. Tillack, Solid-State Electron. **60**, 2 (2011).
[26]N. Von Den Driesch, D. Stange, S. Wirths, G. Mussler, B. Holländer, Z. Ikonic, J. M. Hartmann, T. Stoica, S. Mantl, D. Grützmacher, and D. Buca, Chem. Mater. **27**, 4693 (2015).
[27]S. Mukherjee, N. Kodali, D. Isheim, S. Wirths, J. M. Hartmann, D. Buca, D. N. Seidman, and O. Moutanabbir, Phys. Rev. B **95**, 161402 (2017).
[28]S. Koelling, A. Li, A. Cavalli, S. Assali, D. Car, S. Gazibegovic, E. P. A. M. Bakkers, and P. M. Koenraad, Nano Lett. **17**, 599 (2017).
[29]M. P. Moody, L. T. Stephenson, A. V. Ceguerra, and S. P. Ringer, Microsc. Res. Tech. **71**, 542 (2008).
[30]R. W. Olesinski and G. J. Abbaschian, Bull. Alloy Phase Diagrams **5**, 265 (1984).
[31]B. Gault, M. P. Moody, J. M. Cairney, and S. P. Ringer, *Atom Probe Microscopy* (Springer New York, New York, NY, 2012).
[32]Y. Tu, Z. Mao, and D. N. Seidman, Appl. Phys. Lett. **101**, 121910 (2012).
[33]S. Gupta, B. Magyari-Köpe, Y. Nishi, and K. C. Saraswat, J. Appl. Phys. **113**, 073707 (2013).
[34]T. Schmidt, K. Lischka, and W. Zulehner, Phys. Rev. B **45**, 8989 (1992).
[35]U. Kaufmann, M. Kunzer, M. Maier, H. Obloh, A. Ramakrishnan, B. Santic, and P. Schlotter, Appl. Phys. Lett. **72**, 1326 (1998).
[36]S. Assali, J. Greil, I. Zardo, A. Belabbes, M. W. A. de Moor, S. Koelling, P. M. Koenraad, F. Bechstedt, E. P. A. M. Bakkers, and J. E. M. Haverkort, J. Appl. Phys. **120**, 044304 (2016).
[37]E. Burstein, Phys. Rev. **93**, 632 (1954).
[38]A. E.-J. Lim, J. Song, Q. Fang, C. Li, X. Tu, N. Duan, K. K. Chen, R. P.-C. Tern, and T.-Y. Liow, IEEE J. Sel. Top. Quantum Electron. **20**, 405 (2014).
[39]D. Thomson, A. Zilkie, J. E. Bowers, T. Komljenovic, G. T. Reed, L. Vivien, D. Marris-Morini, E. Cassan, L. Virot, J.-M. Fédéli, J.-M. Hartmann, J. H. Schmid, D.-X. Xu, F. Boeuf, P. O'Brien, G. Z. Mashanovich, and M. Nedeljkovic, J. Opt. **18**, 073003 (2016).
[40]C. Sun, M. T. Wade, Y. Lee, J. S. Orcutt, L. Alloatti, M. S. Georgas, A. S. Waterman, J. M. Shainline, R. R. Avizienis, S. Lin, B. R. Moss, R. Kumar, F. Pavanello, A. H. Atabaki, H. M. Cook, A. J. Ou, J. C. Leu, Y.-H. Chen, K. Asanović, R. J. Ram, M. A. Popović, and V. M. Stojanović, Nature **528**, 534 (2015).
[41]N. von den Driesch, D. Stange, S. Wirths, D. Rainko, I. Povstugar, A. Savenko, U. Breuer, R. Geiger, H. Sigg, Z. Ikonic, J.-M. Hartmann, D. Grützmacher, S. Mantl, and D. Buca, Small **13**, 1603321 (2017).
[42]J. Margetis, A. Mosleh, S. A. Ghetmiri, S. Al-Kabi, W. Dou, W. Du, N. Bhargava, S.-Q. Yu, H. Profijt, D. Kohen, R. Loo, A. Vohra, and J. Tolle, Mater. Sci. Semicond. Process. **70**, 38 (2017).
[43]L. Jiang, C. Xu, J. D. Gallagher, R. Favaro, T. Aoki, J. Menéndez, and J. Kouvetakis, Chem. Mater. **26**, 2522 (2014).
[44]D. Stange, N. Von Den Driesch, D. Rainko, S. Roesgaard, I. Povstugar, J.-M. Hartmann, T. Stoica, Z. Ikonić, S. Mantl, D. Grützmacher, and D. Buca, Optica **4**, 185 (2017).
[45]W. Du, S. A. Ghetmiri, J. Margetis, S. Al-Kabi, Y. Zhou, J. Liu, G. Sun, R. A. Soref, J. Tolle, B. Li, M. Mortazavi, and S.-Q. Yu, J. Appl. Phys. **122**, 123102 (2017).